



Photocatalytic activity of Ag₃PO₄ nanoparticle/TiO₂ nanobelt heterostructures

Ruoyu Liu^a, Peiguang Hu^b, Shaowei Chen^{b,*}

^a Shandong Experimental High School, Jinan, Shandong 250001, China

^b Department of Chemistry and Biochemistry, University of California, Santa Cruz, CA 95064, United States

ARTICLE INFO

Article history:

Received 20 March 2012

Received in revised form 5 June 2012

Accepted 11 June 2012

Available online 18 June 2012

Keywords:

Ag₃PO₄ nanoparticle

TiO₂ nanobelt

Photocatalysis

Methyl orange

ABSTRACT

Heterostructures based on Ag₃PO₄ nanoparticles and TiO₂ nanobelts were prepared by a coprecipitation method. The crystalline structures were characterized by X-ray diffraction measurements. Electron microscopic studies showed that the Ag₃PO₄ nanoparticles and TiO₂ nanobelts were in intimate contact which might be exploited to facilitate charge transfer between the two semiconductor materials. In fact, the heterostructures exhibited markedly enhanced photocatalytic activity as compared with unmodified TiO₂ nanobelts or commercial TiO₂ colloids in the photodegradation of methyl orange under UV irradiation. This was accounted for by the improved efficiency of interfacial charge separation thanks to the unique alignments of their band structures. Remarkably, whereas the photocatalytic activity of the heterostructure was comparable to that of Ag₃PO₄ nanoparticles alone, the heterostructures exhibited significantly better stability and reusability in repeated tests than the Ag₃PO₄ nanoparticles.

© 2012 Elsevier B.V. All rights reserved.

1. Introduction

The physical and chemical properties of titania (titanium dioxide, TiO₂) have been intensively studied for decades [1–4]. As a relatively inexpensive semiconductor material with nontoxicity, long-term stability and chemical inertness in aqueous solutions [5], TiO₂ shows great prospects as a photocatalyst, in particular, for the degradation of organic pollutants in aqueous solutions. The earliest work of titania photocatalysis was reported in 1921 by Renz [6], where it was found that titania turned from white to a dark color under sunlight illumination in the presence of organic compounds such as glycerol. Photocatalytic activity of TiO₂ was also demonstrated by Fujishima and Honda [2] where they used TiO₂ for water splitting, an important process for solar energy conversion.

Nevertheless, the photocatalytic efficiency of TiO₂ alone is generally very low. This is primarily attributed to its wide band gap (~3.2 eV in anatase phase and ~3.0 eV in rutile phase) such that TiO₂ only absorbs lights in the UV region, and thus it is challenging for practical applications with lights in the visible range as the source of excitation energy [1–4]. Furthermore, the high recombination rate of the photo-generated electron/hole pairs also limits the efficiency of TiO₂-based photocatalysts. Therefore, substantial efforts have been devoted to engineering the TiO₂ crystalline and morphological structures for the improvement of the photocatalytic activity. For instance, one-dimensional TiO₂ nanostructures, such as nanowires, nanotubes, and nanobelts, have attracted

significant attention because of their relatively large specific surface areas that may lead to a marked improvement of the photocatalytic activity [7–12]. In addition, doping of transition metals and their oxides or salts onto the surface of the TiO₂ photocatalysts has also been exploited as an effective route to improve the efficiency and range of photo absorption and hence the photocatalytic performance [13–16].

Within this context, Ag₃PO₄ emerges as a promising doping candidate. A recent study by Yi et al. [17] has shown that Ag₃PO₄ can harness visible light and exhibit apparent photocatalytic activity in water splitting as well as degradation of organic contaminants, suggesting effective separation of the photogenerated electrons and holes. However, the lack of chemical stability of Ag₃PO₄ is detrimental to its long-term applications. In addition, the photocatalytic activity in the UV range has remained largely unexplored. It is within this context that the present study was designed and carried out.

In this study, we deposited Ag₃PO₄ particles onto TiO₂ nanobelt surfaces and the resulting composite heterostructures exhibited much enhanced chemical stability in photocatalytic reactions under UV irradiation. We used the photodegradation of methyl orange as the measuring yardstick. The results showed that the UV photocatalytic activity of the Ag₃PO₄/TiO₂ heterostructures was comparable to that of Ag₃PO₄ nanoparticles alone, but was markedly better than the performance of unmodified TiO₂ nanobelts. In addition, the stability and hence reusability of the Ag₃PO₄/TiO₂ heterostructure catalysts was substantially enhanced as compared with that of Ag₃PO₄ nanoparticles or TiO₂ nanobelts alone. These observations might be accounted for by the improved charge separation of the photogenerated electrons and holes under

* Corresponding author. Tel.: +1 831 459 5841; fax: +1 831 459 2935.
E-mail address: shaowei@ucsc.edu (S. Chen).

UV light at the $\text{Ag}_3\text{PO}_4/\text{TiO}_2$ interface and/or surfactant-like function of the nanobelts in stabilizing the Ag_3PO_4 nanoparticles.

2. Experimental

2.1. Chemicals

The raw materials used in this work, including titania P-25 (TiO_2 , ca. 80% anatase, and 20% rutile), sodium hydroxide (NaOH), hydrochloric acid (HCl), sulfuric acid (H_2SO_4), and methyl orange were all purchased from Sinopharm Chemical Reagents Co. Ltd. without further purification or other treatments.

2.2. Preparation of TiO_2 nanobelts

TiO_2 nanobelts were prepared by a hydrothermal process in alkaline solution, as detailed previously [14]. In a typical reaction, 0.5 g of commercial titania P-25 (TiO_2 ; ca. 80% anatase, and 20% rutile) was added into 48 mL of 10 M NaOH aqueous solution and hydrothermally treated at 200 °C in a 60 mL Teflon-lined autoclave for 48 h. After the product was rinsed thoroughly with deionized water, sodium titanate nanobelts were obtained. The sodium titanate nanobelts were then dispersed in a 0.1 M HCl aqueous solution and kept at room temperature. After 48 h the product was rinsed with deionized water again, affording hydrogen titanate nanobelts. The titanate nanobelts were then immersed in 48 mL of 0.02 M H_2SO_4 aqueous solution and filled into a 60 mL Teflon autoclave to be hydrothermally treated at 100 °C for 12 h in order to induce acid corrosion. After the treatment, the nanobelts were extracted from the solution by suction filtration and extensively washed with deionized water. The corroded titanate nanobelts were finally annealed at 600 °C for 2 h, which were denoted as corroded TiO_2 nanobelts.

2.3. $\text{Ag}_3\text{PO}_4/\text{TiO}_2$ nanobelt heterostructures

A coprecipitation method was employed to prepare $\text{Ag}_3\text{PO}_4/\text{TiO}_2$ nanobelt heterostructures with the $\text{Ag}_3\text{PO}_4/\text{TiO}_2$ weight ratio ranging from 1:50 to 2:5. For example, for the 1:10 sample, 0.2 g of TiO_2 nanobelts were added into 50 mL of deionized water and dispersed under ultrasonication, and then 287 μL of 0.5 M AgNO_3 was added into the mixture. The mixture was stirred vigorously for 10 min, and then the pH of the mixture was adjusted to 5 by adding an appropriate amount of 0.1 M nitric acid. A sufficient amount of 0.1 M Na_2HPO_4 was then dripped slowly into the mixture until no change of the color of the mixture was observed. The mixture was then stirred for 20 min and washed thoroughly with deionized water. The nanobelts were separated from the solution by suction filtration, and were dried at 80 °C overnight. A similar procedure was used to prepare Ag_3PO_4 nanoparticles by dripping 0.1 M Na_2HPO_4 slowly into 0.1 M AgNO_3 solution.

2.4. Spectroscopy

X-ray diffraction (XRD) studies were carried out with a Bruke D8 Advance powder X-ray diffractometer with $\text{Cu K}\alpha$ ($\lambda = 0.15406$ nm). A Hitachi S-4800 field-emission scanning electron microscope (FE-SEM) was used to characterize the morphology and size of the prepared catalysts, while energy-dispersive X-ray spectroscopic (EDS) study was performed to characterize the chemical composition of the samples. A JEOL JEM 2100 transmission electron microscope was used to acquire high-resolution TEM images. The UV–vis diffuse reflectance spectra (DRS) of the samples were recorded by a Shimadzu UV-2550 UV–vis spectrophotometer with

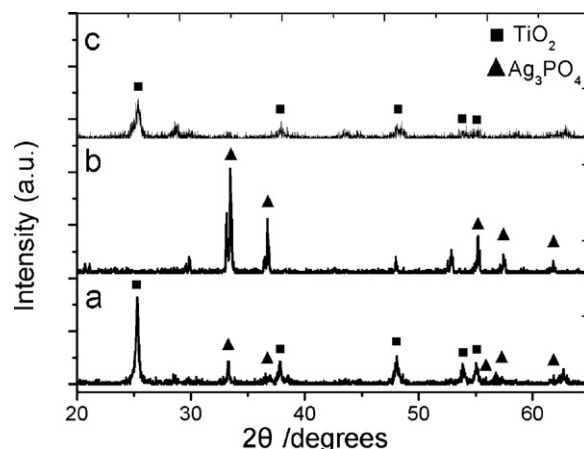


Fig. 1. XRD patterns of (a) $\text{Ag}_3\text{PO}_4/\text{TiO}_2$ (1:10) nanobelt heterostructures, (b) Ag_3PO_4 nanoparticles, and (c) corroded TiO_2 nanobelts.

an integrating sphere attachment, within the wavelength range of 200–650 nm. BaSO_4 was used as a reflectance standard.

2.5. Photocatalysis

Methyl orange (MO) was used as a model compound to examine the photocatalytic activity of the varied samples prepared herein. In a typical experiment, 20 mL of a MO aqueous solution (20 mg/L) and 20 mg of photocatalysts were mixed and put into a 50 mL quartz test tube. The photocatalysts were ultrasonically dispersed in the test tube, and the mixture was then stirred for approximately 5 min. After this treatment, the test tubes were exposed to photoirradiation and stirred synchronously. A 300 W Hg arc lamp was used as the UV light source. The test tubes were then taken away from the light source after designated time intervals and the mixtures were centrifuged to remove the catalysts. The remaining MO concentrations were recorded by a Hitachi UV-3100 UV–vis spectrophotometer.

3. Results and discussion

Fig. 1 shows the representative XRD patterns of the $\text{Ag}_3\text{PO}_4/\text{TiO}_2$ (1:10) nanobelt heterostructures, Ag_3PO_4 nanoparticles and corroded TiO_2 nanobelts. For the unmodified TiO_2 nanobelts (curve c), a series of diffraction peaks can be identified (■), which are consistent with those of anatase TiO_2 (JCPDS 21-1272): 25.7°, 37.0°, 47.9°, 53.7°, and 55.0°, corresponding to the diffractions from the (1 0 1), (0 0 4), (2 0 0), (1 0 5), and (2 1 1) crystal planes of anatase TiO_2 , respectively. These features are also well-defined in the $\text{Ag}_3\text{PO}_4/\text{TiO}_2$ (1:10) heterostructures (curve a), indicating the preservation of the anatase characteristics of the titania support. The diffraction peaks for Ag_3PO_4 nanoparticles are marked with triangles (▲) in curve b at 33.4°, 36.7°, 55.0°, 57.5°, and 61.9°, which may be ascribed to the diffractions from the (2 1 0), (3 1 0), (3 2 0), (3 2 1), and (4 0 0) crystal planes of Ag_3PO_4 , in agreement with those in JCPDS 06-0505. Again, these features are also apparent in the $\text{Ag}_3\text{PO}_4/\text{TiO}_2$ heterostructures (curve a). These observations indicate the successful coupling of the Ag_3PO_4 nanoparticles onto the TiO_2 nanobelt surfaces.

The morphological and microstructural details of the $\text{Ag}_3\text{PO}_4/\text{TiO}_2$ heterostructures were then examined by SEM and HRTEM measurements. Fig. 2(a) depicts the SEM image of TiO_2 nanobelts prepared by the hydrothermal method without acid corrosion. It can be seen that the nanobelts are about 50 nm thick, 50–200 nm wide, and up to a few hundred micrometers long. An acid corrosion treatment led to substantial roughening of the

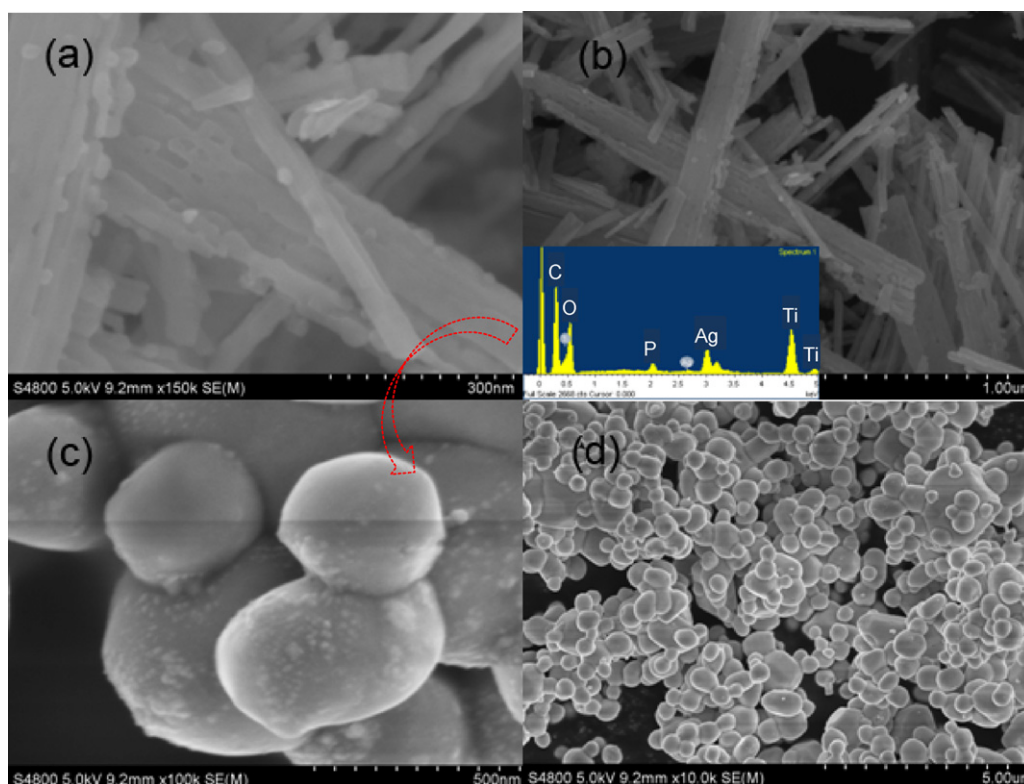


Fig. 2. Representative SEM images of (a) un-corroded TiO_2 nanobelts, (b) corroded TiO_2 nanobelts, (c) $\text{Ag}_3\text{PO}_4/\text{TiO}_2$ (1:10) heterostructures, and (d) Ag_3PO_4 nanoparticles. Inset shows the EDS spectrum of the $\text{Ag}_3\text{PO}_4/\text{TiO}_2$ (1:10) heterostructures where the elements of Ti, O, Ag and P can be clearly identified.

nanobelt surface, as manifested in Fig. 2(b). Such a behavior has been observed previously [18]. It is likely that these roughened surface sites served as the anchoring points for the growth of Ag_3PO_4 nanoparticles by co-precipitation of Ag^+ and PO_4^{3-} in the solution, leading to the generation of $\text{Ag}_3\text{PO}_4/\text{TiO}_2$ heterostructures, as depicted in Fig. 2(c). One can see that the Ag_3PO_4 nanoparticles, with the diameter between 10 and 50 nm (consistent with the TEM measurements as shown below), were deposited onto the roughened TiO_2 surface. Elemental analysis based on energy dispersive X-ray spectroscopy (EDS) measurements was included as the inset to the figure, where the elements of Ti, O, Ag and P can be clearly identified.

As a control experiment, Ag_3PO_4 nanoparticles were also prepared without the TiO_2 nanobelt support, under the otherwise identical experimental conditions. The majority of the nanoparticles exhibited a spherical shape with the diameter around 500 nm, as shown in Fig. 2(d).

Further structural analysis of the $\text{Ag}_3\text{PO}_4/\text{TiO}_2$ heterostructures was carried out by HRTEM measurements. As depicted in Fig. 3, the lattice fringes of both Ag_3PO_4 and TiO_2 can be clearly identified. The former exhibits a lattice constant of about 0.66 nm, consistent with that observed with body-centered cubic Ag_3PO_4 [19], whereas a lattice spacing of 0.35 nm was observed with the TiO_2 nanobelts, in agreement with the spacing of anatase TiO_2 (101) lattice planes (ICDD-JCPDS database, 21-1272). Furthermore, one can see that the Ag_3PO_4 nanoparticle was in intimate contact with the TiO_2 nanobelt support. This unique feature endowed structural stability of the $\text{Ag}_3\text{PO}_4/\text{TiO}_2$ heterostructures, as manifested in the photocatalytic tests below.

Notably, the formation of a $\text{Ag}_3\text{PO}_4/\text{TiO}_2$ heterostructure led to a marked enhancement of optical absorption in the visible range. As depicted in Fig. S1 in the Electronic Supplementary Information (ESI), UV–vis diffuse reflectance spectroscopic measurements showed that the acid-corroded TiO_2 nanobelts exhibited an

absorption threshold at about 380 nm, consistent with the bandgap of anatase titania (3.2 eV). Ag_3PO_4 nanoparticles, however, showed apparent absorption upto ca. 500 nm, in agreement with a bandgap of about 2.4 eV [17,20]. In the $\text{Ag}_3\text{PO}_4/\text{TiO}_2$ heterostructures, the absorption edge remained largely unchanged as compared with that of TiO_2 nanobelts alone; however, the absorbance in the visible range (400–700 nm) was enhanced significantly. This observation is in agreement with the composite nature of the $\text{Ag}_3\text{PO}_4/\text{TiO}_2$

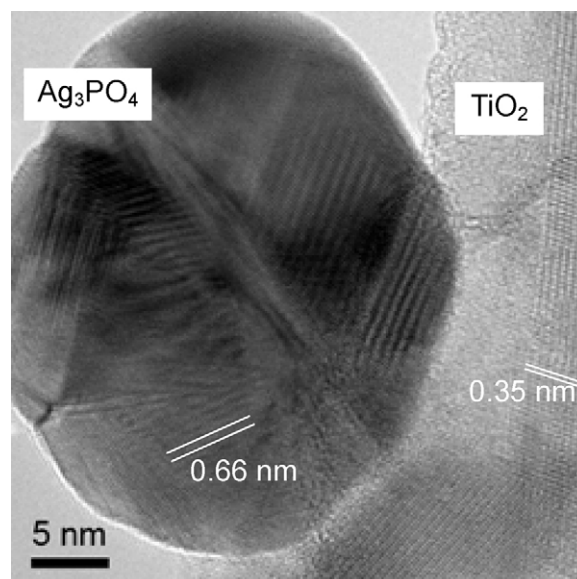


Fig. 3. High resolution images of $\text{Ag}_3\text{PO}_4/\text{TiO}_2$ (1:10) nanobelt heterostructures. White lines highlight the spacing of the TiO_2 and Ag_3PO_4 lattice fringes.

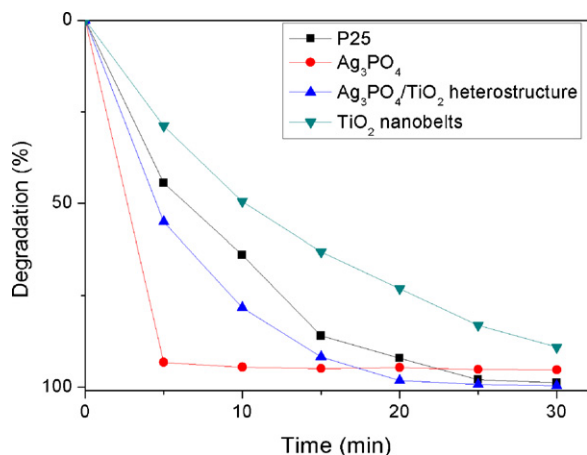


Fig. 4. Comparison of photocatalytic degradation of MO with unmodified corroded TiO₂ nanobelts, Ag₃PO₄ nanoparticles, P25 colloids, Ag₃PO₄/TiO₂ (1:10) nanobellet heterostructures under UV light irradiation.

heterostructures (variations of the Ag₃PO₄/TiO₂ weight ratio did not lead to an apparent difference of the absorption profiles, Fig. S1).

The photocatalytic activity of the Ag₃PO₄/TiO₂ (1:10) heterostructures was then highlighted by the photodegradation of methyl orange in aqueous solutions under UV light irradiation. Fig. 4 shows the decrease of MO absorbance with UV light exposure time in the presence of the Ag₃PO₄/TiO₂ (1:10, ▲) heterostructures. It can be seen that the absorbance and hence the concentration of MO decreases rapidly, and after 20 min of UV exposure, almost 100% of the MO was degraded. Notably, the activity is markedly better than that with unmodified TiO₂ nanobelts (▼), or commercial P25 TiO₂ colloids (■). This observation indicates that the Ag₃PO₄/TiO₂ heterostructures indeed may serve as an effective photocatalyst in the photodegradation of organic dyes.

One may note that the performance of the Ag₃PO₄ nanoparticles (●) appears to be the best among the catalysts tested, with almost 100% of the MO consumed in less than 5 min. However, the Ag₃PO₄ nanoparticles were much less stable than the Ag₃PO₄/TiO₂ heterostructures, which compromised the repeated uses of Ag₃PO₄ in photocatalytic reactions [17]. Fig. 5 compares the photocatalytic activity of the (A) Ag₃PO₄ nanoparticles and (B) Ag₃PO₄/TiO₂ (1:10) heterostructures in MO photodegradation in four runs by using the same catalysts. From panel (A), it can be seen that after the same UV exposure time of 20 min, the amount of MO that had been degraded decreases from 90% to 75%, 70%, and 50% in four repeated cycles, indicating a loss of about 50% of the degradation efficiency of the Ag₃PO₄ nanoparticles. In contrast, the Ag₃PO₄/TiO₂ heterostructures exhibited much enhanced recoverability of the photocatalytic activity. It can be seen from panel (B) that after 20 min of UV exposure, the MO concentration showed a decrease of 88%, 83%, 75%, and 82% in four repeated cycles, where the variation is less than 15%. Further study with varied Ag₃PO₄/TiO₂ weight ratios showed that the optimal loading of Ag₃PO₄ was 1:10 (Fig. S2, ESI).

The results presented above suggest that whereas Ag₃PO₄ nanoparticles exhibited a somewhat better photocatalytic performance in the short term, the Ag₃PO₄/TiO₂ heterostructures appeared to be more desirable in repeated and/or long-term applications because of its enhanced chemical stability. The improved photocatalytic performance of the Ag₃PO₄/TiO₂ heterostructures as compared to that of the unmodified TiO₂ nanobelts or commercial TiO₂ colloids may be accounted for by the electronic band structures of the composite catalysts, which is depicted in Fig. 6. Note that the conduction and valence bands of anatase TiO₂ occur at ca. -4.34 and -7.44 eV, respectively [21]; and for Ag₃PO₄, the valence band maximum (-7.34 eV) is very close to that of anatase

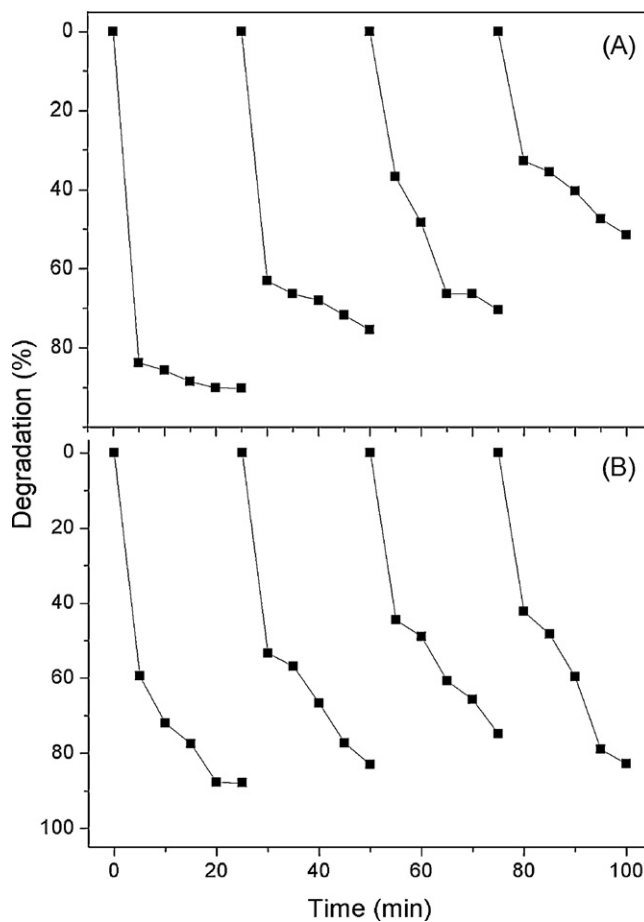


Fig. 5. Photocatalytic activity of (a) Ag₃PO₄ and (b) Ag₃PO₄/TiO₂ (1:10) heterostructures under UV irradiation in repetitive experiments of MO degradation.

TiO₂, whereas the conduction band lies at about -4.9 eV [17]. Under UV photoirradiation, electrons in both Ag₃PO₄ and TiO₂ would be excited from the valence band to the conduction band. On Ag₃PO₄, this would most likely lead to the reduction of Ag(I) into metallic Ag particles [17]. Because of their large Helmholtz double-layer capacitance, metal nanoparticles are generally good electron sinks that may facilitate the interfacial transfer of the TiO₂ photoelectrons to the Ag₃PO₄ conduction band [22]. The holes that remained on both TiO₂ and Ag₃PO₄ then served as powerful oxidizing reagents for the degradation of methyl orange.

Such a band structure (Fig. 6) may also account for the enhanced stability of the Ag₃PO₄/TiO₂ heterostructures, in comparison with Ag₃PO₄ nanoparticles alone. Since the TiO₂ valence band is situated slightly lower than that of Ag₃PO₄, effective hole transport from TiO₂ to Ag₃PO₄ might also occur, leading to the re-oxidation

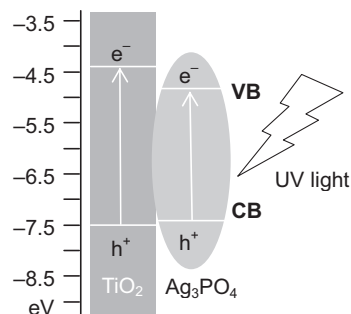


Fig. 6. Schematic of the energy band structure of Ag₃PO₄/TiO₂ heterostructures.

of metallic silver to Ag(I). It is likely that such synergistic interfacial charge transport was facilitated by the intimate contact between the two semiconductor materials, as revealed in electron microscopic measurements (Figs. 2 and 3). Further contributions might arise from the surfactant-like function of the TiO₂ nanobelts for the structural stabilization of the Ag₃PO₄ nanoparticles.

4. Conclusions

Functional heterostructures based on Ag₃PO₄ nanoparticles and TiO₂ nanobelts were prepared by a coprecipitation method, as manifested in X-ray diffraction measurements. Electron microscopic studies showed that the two components were in intimate contact, which might help facilitate interfacial charge transfer during photocatalytic reactions. The photocatalytic activity of the resulting Ag₃PO₄/TiO₂ heterostructures under UV irradiation was examined by using methyl orange as the molecular probe. Experimental results showed that whereas the photocatalytic activity of the heterostructures was comparable to that of Ag₃PO₄ nanoparticles, the structural stability and hence reusability was substantially improved. Furthermore, in comparison with unmodified TiO₂ nanobelts and commercial TiO₂ colloids, the photocatalytic efficiency as well as reusability was both enhanced markedly. The improved performance of the Ag₃PO₄/TiO₂ heterostructures was most likely attributed to the efficient separation of photogenerated electrons and holes, according to the unique alignments of their electronic band structures.

Acknowledgments

This work was supported, in part, by the National Science Foundation (CHE-1012256 and DMR-0804049) and by the ACS-Petroleum Research Fund (49137-ND10). TEM work was performed as a User Project at the National Center for Electron Microscopy, Lawrence Berkeley National Laboratory, which is supported by the US Department of Energy.

Appendix A. Supplementary data

Supplementary data associated with this article can be found, in the online version, at <http://dx.doi.org/10.1016/j.apsusc.2012.06.033>.

References

- [1] A. Fujishima, K. Honda, S. Kikuchi, Photosensitized electrolytic oxidation on TiO₂ semiconductor electrode, *Journal of the Chemical Society of Japan* 72 (1969) 108–113.

- [2] A. Fujishima, K. Honda, Electrochemical photolysis of water at a semiconductor electrode, *Nature* 238 (1972) 37.
- [3] S.A. Bilmes, P. Mandelbaum, F. Alvarez, N.M. Victoria, Surface and electronic structure of titanium dioxide photocatalysts, *Journal of Physical Chemistry B* 104 (2000) 9851–9858.
- [4] X. Chen, S.S. Mao, Titanium dioxide nanomaterials: synthesis, properties, modifications, and applications, *Chemical Reviews* 107 (2007) 2891–2959.
- [5] A. Fujishima, T.N. Rao, D.K. Tryk, Titanium dioxide photocatalysis, *Journal of Photochemistry and Photobiology C: Photochemistry Reviews* 1 (2000) 1–21.
- [6] C. Renz, Light reactions of the oxides of titanium, cerium and earth acids, *Helvetica Chimica Acta* 4 (1921) 961–968.
- [7] T. Kasuga, M. Hiramatsu, A. Hoson, T. Sekino, K. Niihara, Formation of titanium oxide nanotube, *Langmuir* 14 (1998) 3160–3163.
- [8] O.K. Varghese, D.W. Gong, M. Paulose, C.A. Grimes, E.C. Dickey, Crystallization and high-temperature structural stability of titanium oxide nanotube arrays, *Journal of Materials Research* 18 (2003) 156–165.
- [9] B.D. Yao, Y.F. Chan, X.Y. Zhang, W.F. Zhang, Z.Y. Yang, N. Wang, Formation mechanism of TiO₂ nanotubes, *Applied Physics Letters* 82 (2003) 281–283.
- [10] G.K. Mor, K. Shankar, M. Paulose, O.K. Varghese, C.A. Grimes, Use of highly-ordered TiO₂ nanotube arrays in dye-sensitized solar cells, *Nano Letters* 6 (2006) 215–218.
- [11] L.K. Tan, M.K. Kumar, W.W. An, H. Gao, Transparent, well-aligned TiO₂ nanotube arrays with controllable dimensions on glass substrates for photocatalytic applications, *ACS Applied Materials & Interfaces* 2 (2010) 498–503.
- [12] X.W. Kang, S.W. Chen, Photocatalytic reduction of methylene blue by TiO₂ nanotube arrays: effects of TiO₂ crystalline phase, *Journal of Materials Science* 45 (2010) 2696–2702.
- [13] J.H. Park, S. Kim, A.J. Bard, Novel carbon-doped TiO₂ nanotube arrays with high aspect ratios for efficient solar water splitting, *Nano Letters* 6 (2006) 24–28.
- [14] W.J. Zhou, H. Liu, J.Y. Wang, D. Liu, G.J. Du, J.J. Cui, Ag(2)O/TiO(2) nanobelts heterostructure with enhanced ultraviolet and visible photocatalytic activity, *ACS Applied Materials & Interfaces* 2 (2010) 2385–2392.
- [15] C.C. Chen, X.Z. Li, W.H. Ma, J.C. Zhao, H. Hidaka, N. Serpone, Effect of transition metal ions on the TiO₂-assisted photodegradation of dyes under visible irradiation: a probe for the interfacial electron transfer process and reaction mechanism, *Journal of Physical Chemistry B* 106 (2002) 318–324.
- [16] Q. Li, M.A. Page, B.J. Marinas, J.K. Shang, Treatment of coliphage MS2 with palladium-modified nitrogen-doped titanium oxide photocatalyst illuminated by visible light, *Environmental Science & Technology* 42 (2008) 6148–6153.
- [17] Z.G. Yi, J.H. Ye, N. Kikugawa, T. Kako, S.X. Ouyang, H. Stuart-Williams, H. Yang, J.Y. Cao, W.J. Luo, Z.S. Li, Y. Liu, R.L. Withers, An orthophosphate semiconductor with photooxidation properties under visible-light irradiation, *Nature Materials* 9 (2010) 559–564.
- [18] P.G. Hu, G.J. Du, W.J. Zhou, J.J. Cui, J.J. Lin, H. Liu, D. Liu, J.Y. Wang, S.W. Chen, Enhancement of ethanol vapor sensing of TiO(2) nanobelts by surface engineering, *ACS Applied Materials & Interfaces* 2 (2010) 3263–3269.
- [19] H.N. Ng, C. Calvo, R. Faggiani, New investigation of structure of silver orthophosphate, *Acta Crystallographica Section B-Structural Science* 34 (1978) 898–899.
- [20] A. Fujishima, X.T. Zhang, D.A. Tryk, TiO(2) photocatalysis and related surface phenomena, *Surface Science Reports* 63 (2008) 515–582.
- [21] A.J. Nozik, R. Memming, Physical chemistry of semiconductor–liquid interfaces, *Journal of Physical Chemistry* 100 (1996) 13061–13078.
- [22] S. Pradhan, D. Ghosh, S.W. Chen, Janus nanostructures based on Au-TiO₂ heterodimers and their photocatalytic activity in the oxidation of methanol, *ACS Applied Materials & Interfaces* 1 (2009) 2060–2065.